

THE ROLE OF TINY GRAINS ON THE ACCRETION PROCESS IN PROTOPLANETARY DISKS

XUE-NING BAI

Department of Astrophysical Sciences, Princeton University, Princeton, NJ, 08544
Draft version August 25, 2021

ABSTRACT

Tiny grains such as polycyclic aromatic hydrocarbons (PAHs) have been thought to dramatically reduce the coupling between gas and magnetic fields in weakly ionized gas such as in protoplanetary disks (PPDs) because they provide tremendous surface area to recombine free electrons. The presence of tiny grains in PPDs thus raises the question of whether the magnetorotational instability (MRI) is able to drive rapid accretion to be consistent with observations. Charged tiny grains have similar conduction properties as ions, whose presence leads to qualitatively new behaviors in the conductivity tensor, characterized by $\bar{n}/n_e > 1$, where n_e and \bar{n} denote the number densities of free electrons and all other charged species respectively. In particular, Ohmic conductivity becomes dominated by charged grains rather than electrons when \bar{n}/n_e exceeds about 10^3 , and Hall and ambipolar diffusion (AD) coefficients are reduced by a factor of $(\bar{n}/n_e)^2$ in the AD dominated regime relative to that in the Ohmic regime. Applying the methodology of Bai (2011), we find that in PPDs, when PAHs are sufficiently abundant ($\gtrsim 10^{-9}$ per H₂ molecule), there exists a transition radius r_{trans} of about 10–20 AU, beyond which the MRI active layer extends to the disk midplane. At $r < r_{\text{trans}}$, the optimistically predicted MRI-driven accretion rate \dot{M} is one to two orders of magnitude smaller than that in the grain-free case, which is too small compared with the observed rates, but is in general no smaller than the predicted \dot{M} with solar-abundance $0.1\mu\text{m}$ grains. At $r > r_{\text{trans}}$, we find that remarkably, the predicted \dot{M} exceeds the grain-free case due to a net reduction of AD by charged tiny grains, and reaches a few times $10^{-8}M_{\odot}\text{yr}^{-1}$. This is sufficient to account for the observed \dot{M} in transitional disks. Larger grains ($\gtrsim 0.1\mu\text{m}$) are too massive to reach such high abundance as tiny grains and to facilitate the accretion process.

Subject headings: accretion, accretion disks — instabilities — magnetohydrodynamics (MHD) — protoplanetary disks — turbulence

1. INTRODUCTION

Weakly ionized gas is not perfectly conducting. In the presence of magnetic field (\mathbf{B}), the Ohm's law is anisotropic, giving rise to Ohmic resistivity, Hall effect, and ambipolar diffusion (AD) as the three non-ideal magnetohydrodynamics (MHD) effects. More formally, assuming the inertia in the ionized species is negligible, the dynamical equations for the neutrals are the same as ideal MHD except for the induction equation, which reads

$$\frac{\partial \mathbf{B}}{\partial t} = \nabla \times (\mathbf{v} \times \mathbf{B}) - \frac{4\pi}{c} \nabla \times [\eta_O \mathbf{J} + \eta_H (\mathbf{J} \times \hat{\mathbf{B}}) + \eta_A \mathbf{J}_{\perp}], \quad (1)$$

where \mathbf{v} is the velocity of the neutrals, $\mathbf{J} = (c/4\pi)\nabla \times \mathbf{B}$ is the current density, $\hat{\mathbf{B}}$ denotes unit vector along \mathbf{B} , subscript “ \perp ” denotes the vector component that is perpendicular to \mathbf{B} , η_O , η_H and η_A are the Ohmic, Hall and the ambipolar diffusivities, which depend on the number density of the charged species, and the latter two also depend on B . When ions and electrons are the only charged species in the gas (which can be relaxed to when the electrons are the main negative charge carriers), a simple expression for the diffusion coefficients

reads (Salmeron & Wardle 2003):

$$\eta_O = \eta_e, \quad \eta_H = \frac{cB}{4\pi en_e}, \quad \eta_A = \frac{B^2}{4\pi\gamma_i\rho\rho_i}, \quad (2)$$

where η_e is the resistivity due to the electrons, n_e is the electron number density, ρ and ρ_i are the mass density of the neutrals and the ions, γ_i is defined after equation (4). In general, Ohmic effect dominates in dense regions with weak magnetic field, AD dominates in tenuous regions with strong magnetic field, while the Hall regime lies in between.

Grains, which typically contribute to about $\lesssim 1\%$ of mass in the gas, can possess both positive and negative charges. Grains are well known for significantly enhancing the electron recombination rate (Draine & Sutin 1987), which reduces the ionization fraction (n_e/n_H , where n_H is the number density of hydrogen atom), and leads to greatly increased Ohmic resistivity. However, in sufficiently weakly ionized gas, the abundance of tiny grains (e.g., the polycyclic aromatic hydrocarbon, PAH) may well exceed the electron abundance without contributing much to the mass budget. In this paper, we generalize equation (2) to include positive and negatively charged tiny grains and show that for sufficiently weak ionization, tiny grains can dramatically reduce η_H and η_A as the main charge carrier switches to the grains instead of ions and electrons.

Our result is directly applicable to protoplanetary disks

arXiv:1107.2936v1 [astro-ph.EP] 14 Jul 2011

(PPDs), where the ionization fraction resulting from major ionization sources such as X-rays and cosmic rays is generally orders of magnitude below unity, and it decreases from surface to the midplane because of the attenuation of ionizing particles (Gammie 1996). Non-ideal MHD effects are closely relevant to the magnetorotational instability (MRI, Balbus & Hawley 1991), whose linear dispersion relation as well as the non-linear saturation properties are strongly affected (Wardle 1999; Balbus 2009), and whether the MRI is responsible for driving rapid accretion with $\dot{M} \sim 10^{-8\pm 1} M_{\odot} \text{ yr}^{-1}$ in PPDs (Hartmann et al. 1998) has been a long-standing problem. Most studies have focused on the role of the Ohmic resistivity (e.g., Turner et al. 2007; Bai & Goodman 2009), while it was not until recently have AD been taken into account to estimate the effectiveness of the MRI (Chiang & Murray-Clay 2007; Perez-Becker & Chiang 2011a). Combining the most recent results from numerical simulations of the MRI with AD (Bai & Stone 2011), Bai (2011) showed that while the MRI can always operate in PPDs, AD can be a main limiting factor for the MRI-driven accretion (besides Ohmic resistivity). The reduction of AD coefficient by tiny grains (e.g., PAHs), while counterintuitive, helps enhance the accretion rate, as we will demonstrate in this paper.

Although observational data show strong evidence of grain growth to micron size or larger in PPDs (e.g., D'Alessio et al. 2001; van Boekel et al. 2003), PAH emission has also been detected in majority of Herbig Ae/Be stars (Acke & van den Ancker 2004), as well as a small fraction of T-Tauri stars (Geers et al. 2006; Oliveira et al. 2010). As argued in Perez-Becker & Chiang (2011a), PAHs may be equally abundant in T-Tauri disks but they fluoresce less luminously due to fainter ultraviolet radiation field of their host stars. The existence of PAHs also suggests a continuous size distribution of grains to the smallest end of a few Å as a result of grain coagulation and fragmentation. Throughout this paper, we use the phrases “tiny grain” and PAH interchangeably, which refer to grain with size $a \lesssim 0.01 \mu\text{m}$. Tiny grains may dominate larger grains in abundance while contribute a negligible fraction of the total grain mass. Taking the grain density to be 3 g cm^{-3} and the gas mean molecular weight μ_n to be 2.34 atomic mass (as appropriate for PPDs), the relation between grain mass fraction (f) and grain abundance per H_2 molecule (x) reads

$$\frac{f}{0.01} \approx 0.32 \left(\frac{x}{10^{-9}} \right) \left(\frac{a}{0.01 \mu\text{m}} \right)^3, \quad (3)$$

where a is grain size. The abundance of grains with $a \lesssim 0.01 \mu\text{m}$ may easily reach large abundance of 10^{-9} or higher, while the abundance of $a \gtrsim 0.1 \mu\text{m}$ grains would be at most about 10^{-12} . The significance of this abundance cut ($x = 10^{-9}$) will be addressed in this paper.

In Section 2 we describe a generalized model for non-ideal MHD diffusion coefficients with the inclusion of charged grains. The model is applied to interpret the results in Section 3, where we study the role of tiny grains in PPDs following the methodology of Bai (2011). Summary and discussion follow in Section 4.

2. NON-IDEAL MHD EFFECTS WITH GRAINS

The Ohm's Law derives from the motion of charged particles, which is characterized by the Hall parameter, the ratio between the gyrofrequency and the momentum exchange rate (Wardle 2007). For species j with mass m_j and charge $Z_j e$, the Hall parameter reads

$$\beta_j \equiv \frac{|Z_j| e B}{m_j c} \frac{1}{\gamma_j \rho}. \quad (4)$$

where $\gamma_j \equiv \langle \sigma v \rangle_j / (\mu_n + m_j)$ with $\langle \sigma v \rangle_j$ being the rate coefficient for momentum transfer between charged species j with the neutrals and μ_n is the mean molecular weight of the neutrals. Charged species j is strongly coupled to the neutrals if $|\beta_j| \ll 1$, and is strongly tied to magnetic fields when $|\beta_j| \gg 1$.

In weakly ionized gas with a number of different charged species, the general expressions for the Ohmic, Hall and ambipolar diffusion coefficients are given by (Wardle 2007; Bai 2011)

$$\begin{aligned} \eta_O &= \frac{c^2}{4\pi\sigma_O}, \\ \eta_H &= \frac{c^2}{4\pi\sigma_{\perp}} \frac{\sigma_H}{\sigma_{\perp}}, \\ \eta_A &= \frac{c^2}{4\pi\sigma_{\perp}} \frac{\sigma_P}{\sigma_{\perp}} - \eta_O, \end{aligned} \quad (5)$$

where $\sigma_{\perp} \equiv \sqrt{\sigma_H^2 + \sigma_P^2}$ and the Ohmic, Hall and Pedersen conductivities are

$$\begin{aligned} \sigma_O &= \frac{ec}{B} \sum_j n_j |Z_j| \beta_j, \\ \sigma_H &= \frac{ec}{B} \sum_j \frac{n_j Z_j}{1 + \beta_j^2}, \\ \sigma_P &= \frac{ec}{B} \sum_j \frac{n_j |Z_j| \beta_j}{1 + \beta_j^2} \end{aligned} \quad (6)$$

respectively, where the summation goes over all charged species. Note that the Hall conductivity depends on the sign of Z_j , while σ_O and σ_P depend only on $|Z_j|$.

The simple expressions for the magnetic diffusion coefficients (2) can be obtained by assuming electrons and ions are the only two charged species. Below we generalize it to include tiny grains. Besides the reason mentioned in the introduction, we consider tiny grains because they are unlikely to possess multiple charges due to higher potential barrier (Perez-Becker & Chiang 2011a), which simplifies the algebra considerably. In addition, the mean free path for tiny grains is sufficiently small so that they can be treated as fluid.

The momentum transfer rate coefficients for electrons, ions and grains can be found in equations (14) - (16) of Bai (2011). Converting to the Hall parameter, we have

$$\begin{aligned} \beta_i &\approx 3.3 \times 10^{-3} \frac{B_G}{n_{15}}, \\ \beta_e &\approx 2.1 \frac{B_G}{n_{15}} \max \left[1, \left(\frac{T}{100\text{K}} \right)^{1/2} \right] \gg \beta_i, \end{aligned} \quad (7)$$

for ions and electrons respectively, where B_G is the magnetic field strength measured in Gauss, $n_{15} = n_H / 10^{15}$

cm^{-3} , and the μ_n is taken to be 2.34 atomic mass appropriate for PPDs. For singly charged small grains, the resulting β is very close to β_i , because the reduced gyro-frequency due to larger mass is compensated by the reduced momentum transfer rate due to larger inertia. The electron Hall parameter β_e is much larger than β_i because electrons are the most mobile species. Therefore, in terms of conductivity, we only have two groups of charges: electrons with Hall parameter β_e , and ions / charged grains with Hall parameter β_i .

Let $\bar{n} = n_i + n_{\text{gr}}^+ + n_{\text{gr}}^-$ be the total number density of the second group. Since grains can carry negative charge, one has $\bar{n} \geq n_e$. Generalization from $\bar{n} = n_e$ (grain-free case, which leads to equation (2)) to $\bar{n} > n_e$ involves more complicated algebra, as we describe below. For brevity, we ignore the pre-factor $en_e c/B$ in conductivities and $cB/4\pi en_e$ in diffusivities, which make them dimensionless.

The three components of the conductivity tensor read

$$\begin{aligned}\sigma_O &= \beta_e + \frac{\bar{n}}{n_e} \beta_i = (\beta_e + \beta_i)(1 + \theta), \\ \sigma_H &= \frac{1}{1 + \beta_e^2} - \frac{1}{1 + \beta_i^2} = \frac{(\beta_e + \beta_i)(\beta_e - \beta_i)}{(1 + \beta_e^2)(1 + \beta_i^2)}, \\ \sigma_P &= \frac{\beta_e}{1 + \beta_e^2} + \frac{(\bar{n}/n_e)\beta_i}{1 + \beta_i^2} = \frac{(\beta_e + \beta_i)}{(1 + \beta_i^2)} \left[\frac{(1 + \beta_e\beta_i)}{(1 + \beta_e^2)} + \theta \right],\end{aligned}\quad (8)$$

where we have defined

$$\theta \equiv \frac{\bar{n} - n_e}{n_e} \frac{\beta_i}{\beta_e + \beta_i} \approx \frac{n_{\text{gr}}^\pm \beta_i}{n_e \beta_e}. \quad (9)$$

The parameter θ is independent of magnetic field, and measure the ratio of grain conductivity to electron conductivity. Note that $\theta = 0$ in the grain-free case, and the Hall conductivity is independent of θ . The perpendicular conductivity is

$$\sigma_\perp^2 = \frac{(\beta_e + \beta_i)^2}{(1 + \beta_e^2)(1 + \beta_i^2)} \frac{1}{f(\theta)}, \quad (10)$$

where

$$f(\theta) \equiv \frac{(1 + \beta_i^2)}{[(1 + \theta)^2 + (\beta_i + \theta\beta_e)^2]}. \quad (11)$$

Note that $f(\theta) = 1$ in the grain-free case ($\theta = 0$). It is straightforward to obtain the Ohmic, Hall and ambipolar diffusion coefficients, after some algebra

$$\eta_O = \frac{1}{(\beta_e + \beta_i)(1 + \theta)} \approx \frac{1}{\beta_e(1 + \theta)}, \quad (12)$$

$$\eta_H = \frac{\beta_e - \beta_i}{\beta_e + \beta_i} f(\theta) \approx f(\theta), \quad (13)$$

$$\begin{aligned}\eta_A &= \frac{[(1 + \theta) + \beta_e(\beta_i + \theta\beta_e)]}{(\beta_e + \beta_i)} f(\theta) - \eta_O \\ &\approx \left[(1 + \theta)(\beta_i + \theta\beta_e) - \frac{\beta_e \theta^2}{1 + \beta_i^2} \right] \frac{f(\theta)}{1 + \theta},\end{aligned}\quad (14)$$

where the approximate formulae are obtained by noting that $\beta_e \gg \beta_i$, with error on the order of $\beta_i/\beta_e \sim 10^{-3}$.

We see that the grains affect the magnetic diffusion coefficients mainly via two factors: $(1 + \theta)$ and $(\beta_i + \theta\beta_e)/\beta_i \approx \bar{n}/n_e$, both of which are independent of magnetic field strength. The former describes the ratio of total conductivity to electron conductivity, while the latter describes the number density ratio of ions / grains to electrons, and is much more substantial than the factor $(1 + \theta)$ since $\beta_e \gg \beta_i$.

For $\theta \ll \beta_i/\beta_e \sim 10^{-3}$, we generally have $\bar{n} \approx n_i \approx n_e$, $f(\theta) \approx 1$, and the classical results (2) are recovered. In particular, Ohmic resistivity dominates when $\beta_e < 1$, where both ions and electrons are coupled to the neutrals; Hall regime corresponds to $\beta_i < 1 < \beta_e$, where electrons are coupled to the magnetic field while the ions are not; AD regime corresponds to $\beta_i > 1$ where both electrons and ions are coupled to the magnetic field. This is the classical interpretation of the non-ideal MHD effects.

Qualitatively new behaviors appear when $\theta \gtrsim \beta_i/\beta_e$, where grains play a dominant role in the abundance of charged particles ($n_{\text{gr}}^\pm \gtrsim n_e$). In the next two paragraphs, we discuss the asymptotic behaviors of the diffusion coefficients, where comparison is made with the grain-free diffusion coefficients (2) at fixed n_e . In reality, tiny grains strongly reduces n_e relative to the grain-free case, which will be discussed at the end of this section.

The Ohmic resistivity is least affected by grains, which is simply reduced by a factor of $(1 + \theta)$ relative to the electron resistivity regardless of magnetic field strength. Therefore, grain conductivity becomes important when $\theta \gtrsim 1$ or $\bar{n} \gtrsim 10^3 n_e$. For Hall and AD coefficients, we consider two separate limits. When $\beta_i \ll \beta_e \ll 1$ (Ohmic regime), we have

$$\begin{aligned}\eta_H &\approx \frac{cB}{4\pi en_e} \frac{1}{(1 + \theta)^2}, \\ \eta_A &\approx \frac{cB\beta_i}{4\pi en_e} \frac{\bar{n}}{n_e(1 + \theta)^3},\end{aligned}\quad (15)$$

where we have factored out the results into the grain-free expression (left) multiplied by a correction factor (right). We see that the Hall diffusivity is only moderately affected by grains, being reduced by a factor of $(1 + \theta)^2$ at fixed n_e . The AD, on the other hand, is enhanced by a factor of \bar{n}/n_e , in addition to a moderate reduction by $(1 + \theta)^3$. Nevertheless, changes in Hall and AD coefficients do not play a significant role here since Ohmic resistivity is still the dominant effect.

In the opposite limit $1 \ll \beta_i \ll \beta_e$ (AD regime), we have

$$\begin{aligned}\eta_H &\approx \frac{cB}{4\pi en_e} \left(\frac{n_e}{\bar{n}} \right)^2, \\ \eta_A &\approx \frac{cB\beta_i}{4\pi en_e} \frac{n_e}{\bar{n}}.\end{aligned}\quad (16)$$

We see that in this limit and at fixed n_e , the Hall effect is reduced by a factor of $(\bar{n}/n_e)^2$, while AD is reduced by a factor of (\bar{n}/n_e) . The reduction of AD is easily understood. Without grains, the neutral gas is coupled to the magnetic field through ion-neutral collisions, hence $\eta_A \propto 1/n_i = 1/n_e$. Electrons play a negligible role because of its small inertia. Charged grains (no matter positive or negative) play exactly the same role as ions,

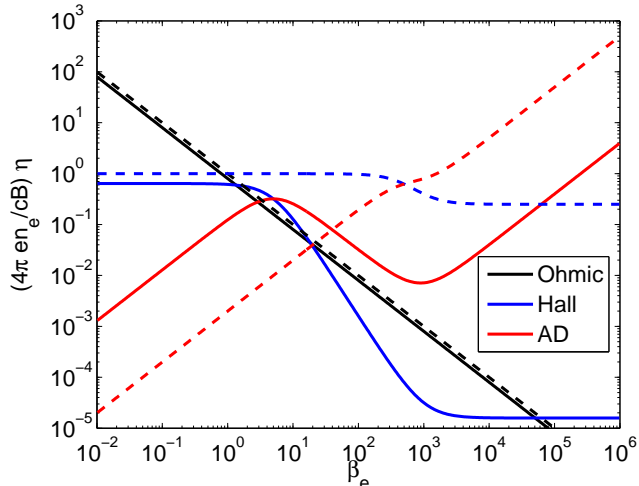


FIG. 1.— Dimensionless Ohmic (black), Hall (blue) and ambipolar (red) diffusion coefficients as a function of the electron Hall parameter $\beta_e = 1000\beta_i$. We have considered two different values of the charged grain abundance parameter: $\theta = 10^{-3}$ ($\bar{n} = 2n_e$, dashed) and $\theta = 0.25$ ($\bar{n} = 251n_e$, solid).

hence we have $\eta_A \propto 1/\bar{n}$ in the presence of grains. We also note that the Hall effect vanishes if positive and negative charge carriers have the same mass, which is consistent with our result as $n_e/\bar{n} \rightarrow 0$.

In Figure 1 we show two sample calculations of the magnetic diffusion coefficients for $\theta = 10^{-3}$ (dashed) and $\theta = 0.25$ (solid) respectively, which corresponds to situations where charged grain abundance is comparable to, and greatly exceed the electron abundance. The two asymptotic regimes derived above are clearly seen, with a transition region in between. The $\theta = 10^{-3}$ results are close to the grain-free case, where all three curves are close to straight lines except weak transitions as β_i passes 1. For relatively large θ , the transition region extends from $\beta_e \approx 1$ to $\beta_i \approx 1$. Because of the suppression of the Hall diffusion beyond $\beta_e \approx 1$ and enhancement of AD before $\beta_e \approx 1$, AD becomes the dominant effect even when $\beta_i \ll 1$ ($\beta_e \ll 1000$), and the Hall regime gradually diminishes as θ increases. These results nicely explain the observed magnetic diffusivity pattern in Figure 2 of Bai (2011), as aided with the chemical abundances shown in Figure 1 of the same paper.

Now let us take into account the chemistry in the gas. Assuming fixed gas density, temperature, and ionization rate, the equilibrium electron number density in the presence of small grains n_{e1} is much smaller than that in the grain-free case n_{e0} (Bai & Goodman 2009; Perez-Becker & Chiang 2011a). Therefore, Hall and AD coefficients are made larger by a factor of n_{e0}/n_{e1} . However, this factor is compensated by another reduction factor of $(n_{e1}/\bar{n})^2$ for the Hall effect and of n_{e1}/\bar{n} for AD in the AD dominated regime. Here we focus on AD. In order to have a net reduction of AD coefficient when $\beta_i \gg 1$ (AD regime), it is required that

$$\bar{n} > n_{e0}. \quad (17)$$

That is, the charged grain abundance has to exceed the grain-free electron abundance. We will see that this condition can be met in PPDs. Similarly, for Ohmic resistivity to be reduced relative to the grain-free case, one

requires $\bar{n} \gtrsim 10^3 n_{e0}$. This condition, however, is very unrealistic given the disk chemistry (see Section 3.1), thus Ohmic resistivity always increases in the presence of tiny grains. Nevertheless, if condition (17) is met (which is generally the case when PAHs are sufficiently abundant, see Section 3.1), Ohmic resistivity is enhanced by at most a factor of about 10^3 relative to the grain-free case.

3. APPLICATION TO THE MAGNETOROTATIONAL INSTABILITY IN PPDs

To illustrate the significance of the theoretical results in the previous section, we study the role of tiny grains in PPDs. We refer to Section 3 of Bai (2011) for all details about the methodology and calculation procedures, which we follow exactly except that here we consider $a = 1$ nm sized grains (as a proxy for PAHs) instead of larger grains¹. The PAH abundance in T-Tauri stars estimated by Geers et al. (2006) is about $x_{\text{PAH}} \approx 10^{-8}$ - 10^{-7} per H_2 molecule, while Perez-Becker & Chiang (2011a) argued for smaller abundance due to dust settling. Moreover, the distribution of PAHs in PPDs has been found to be spatially variable (Geers et al. 2007). For these reasons, we adopt $x_{\text{PAH}} = 10^{-8}$ as fiducial, while we also consider x_{PAH} down to 10^{-11} and up to 10^{-7} . We fix the X-ray luminosity to be $10^{30} \text{ erg s}^{-1}$, X-ray temperature to be 5 keV, and include cosmic-ray ionization of 10^{-17} s^{-1} with penetration depth of 96 g cm^{-2} . We use the minimum-mass solar nebular (MMSN, Hayashi 1981) as the fiducial disk model, while we also consider the much more massive disk model by Desch (2007). A complex chemical network of more than 4000 reactions are evolved at different heights and radii of the disk for 1 Myr to (quasi-) chemical equilibrium, from which abundance of charged species are extracted to evaluate the non-ideal MHD diffusion coefficients. We will mainly focus on the outer disk ($\gtrsim 10 \text{ AU}$) where AD rather than Ohmic resistivity plays the dominant role the gas dynamics and the effect discussed in Section 2 is most relevant.

3.1. Abundance of Charged Species

In Figure 2 we show the electron, ion and grain abundances at 40 AU in the MMSN model as a function of disk height (z), normalized to the disk scale height ($H = c_s/\Omega$ where c_s is the sound speed, Ω is the disk angular frequency). We see that electrons and ions are the dominant charged species (i.e., $\bar{n} \approx n_e$) above $\sim 3H$, while below it the abundances of ions and charged grains exceed electron abundance, and \bar{n}/n_e reaches about 1000 at the disk midplane. The large value of \bar{n}/n_e implies strong suppression of AD and the Hall effect according to equation (16). To see its significance, we also show the electron (thus ion) abundance in the grain-free calculation as the red dash-dotted line in the Figure. Clearly, we see that $n_{e0} < \bar{n}$ for $z \lesssim 2H$. According to equation (17), this means that when tiny grains are present, the AD coefficient is even smaller than that in the grain-free case! Seemingly counterintuitive, one can qualitatively understand this result as follows.

¹ We use binding energy of $D = 3 \text{ eV}$ in the calculation of the electron-grain sticking coefficient rather than 1 eV used in Bai (2011).

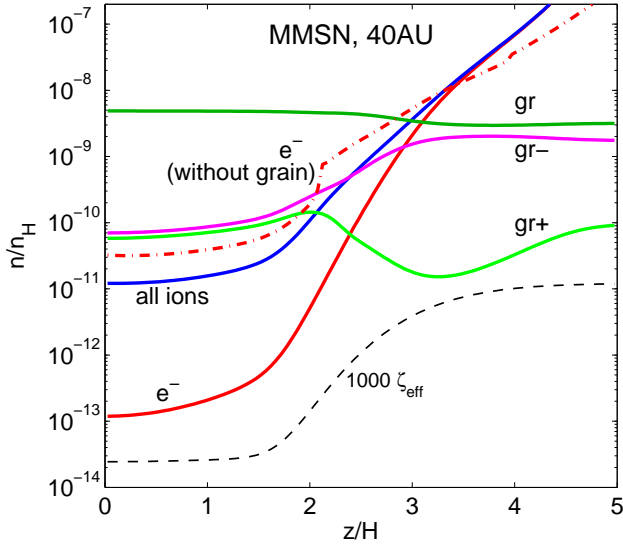


FIG. 2.— Abundance of charged species and grains (PAHs) as a function of disk height in our fiducial model calculation (MMSN disk with $x_{\text{PAH}} = 10^{-8}$) at 40 AU, plotted as solid lines with labels. For comparison, red dash-dotted line shows the electron (and ion) abundance in the grain-free calculation. The ionization rate is plotted (black dashed) for reference.

Near the disk midplane, we see that $n_{\text{gr}} \gg n_{\text{gr}}^{\pm} \gtrsim n_i \gg n_e$. In this regime, the electrons produced from H_2 ionization is quickly swallowed by the grains. Similarly, the ions exchange charge with neutral grains to produce positively charged grains. Therefore, ionization effectively takes place on the grains: $2 \text{gr} \rightarrow \text{gr}^+ + \text{gr}^-$, with the same ionization rate ζ_{eff} . The dominant recombination channel is simply its inverse reaction, with recombination rate given by equation (3) of Umebayashi & Nakano (1990). For recombination between two equal sized tiny grains ($e^2/akT \gg 1$), it reduces to

$$\begin{aligned} \langle \sigma v \rangle_{gg} &\approx \left(\frac{48e^4}{\rho_d akT} \right)^{1/2} \\ &\approx 2.5 \times 10^{-8} a_1^{-1/2} T_{100}^{-1/2} \text{s}^{-1} \text{cm}^3, \end{aligned} \quad (18)$$

where $\rho_d = 3 \text{ g cm}^{-3}$ is the grain mass density, k is the Boltzmann constant, T is the temperature. In the second equation a_1 denotes grain size normalized to 1 nm, and $T_{100} = T/100 \text{ K}$. As long as charged grain recombination is the dominant recombination process, the abundance of charged grains can be approximately given by

$$\begin{aligned} \frac{n_{\text{gr}}^{\pm}}{n_H} &\approx \sqrt{\frac{\zeta_{\text{eff}}}{2\langle \sigma v \rangle_{gg} n_H}} \\ &\approx 1.3 \times 10^{-10} \zeta_{\text{eff},-17}^{1/2} n_{H,10}^{-1/2} a_1^{1/4} T_{100}^{1/4}, \end{aligned} \quad (19)$$

where $\zeta_{\text{eff},-17}$ is the ionization rate normalized to 10^{-17} s^{-1} , $n_{H,10}$ is the number density of the hydrogen atoms normalized to 10^{10} cm^{-3} . Plugging in the numbers relevant to Figure 2 at midplane, we find $n_{\text{gr}}^{\pm}/n_H \approx 1.1 \times 10^{-10}$. Our chemistry calculation gives 6.5×10^{-11} for the averaged abundance of charged grains, which is slightly smaller due to small contributions from other recombination channels, but is within a factor of 2 from

the analytical estimate. Our chemistry calculations further reveal that n_{gr}^{\pm}/n_H increases weakly with total grain abundance n_{gr} (or x_{PAH}) and approaches the asymptotic value (19).

In the grain-free case, the electron abundance n_{e0} is determined by the balance between ionization and multiple recombination channels, dominated by dissociative recombinations. Typical electron-ion dissociative recombination rate coefficients are on the order of $10^{-7} \text{ s}^{-1} \text{ cm}^{-3}$ at 100K, which is a factor of several higher than the grain recombination coefficient (18). The higher recombination rate leads to smaller ionization level than our estimate (19), which explains why $n_{e0} < \bar{n}$ in the presence of abundant tiny grains. We note that the value of n_{e0} depends on the choice of chemical reaction network. Simple reaction network (such as Oppenheimer & Dalgarno 1974) generally produces larger n_{e0} mainly because of the lack of recombination channels. In our complex (and presumably more realistic) network, we find that the dominant recombination process is due to NH_4^+ and CH_3CNH^+ in this particular case, giving n_{e0}/n_H to be about 3.2×10^{-11} . As a result, we obtain $\bar{n}/n_{e0} \approx 4$ in the midplane, which leads to a substantial net reduction of the AD coefficient.

3.2. Active Layer and Accretion Rate

The fact that $\bar{n} > n_{e0}$ implies that tiny grains may facilitate the MRI by suppressing AD. To see this more explicitly, we calculate the non-ideal MHD diffusion coefficients and apply the criteria (20) in Bai (2011) to identify the MRI-active regions in our adopted PPD model. Briefly, for the MRI to operate, the Ohmic Elsasser number $\Lambda \equiv v_A^2/\eta_O\Omega$ has to be greater than unity, where $v_A = B/\sqrt{4\pi\rho}$ is the Alfvén velocity. Moreover, the magnetic field has to be weaker than some critical value, which is set by $\beta \geq \beta_{\text{min}}(Am)$. Here plasma β is the ratio of gas to magnetic pressure (not to be confused with the Hall parameter), $Am \equiv v_A^2/\eta_A\Omega$ is the AD Elsasser number, and $\beta_{\text{min}}(Am)$ is given by (Bai & Stone 2011)

$$\beta_{\text{min}} = \left[\left(\frac{50}{Am^{1.2}} \right)^2 + \left(\frac{8}{Am^{0.3}} + 1 \right)^2 \right]^{1/2}, \quad (20)$$

which increases with decreasing Am . For the number density profile given in Figure 2, the result is shown in Figure 3.

We see that the inclusion of tiny grains strongly increases the Ohmic resistivity, as expected. At disk midplane, magnetic field has to be about 10 times stronger than the grain-free case in order for Λ to be above 1 (i.e., η_O is about 100 times larger²). However, the ionization fraction at disk midplane is still large enough such that in both cases, the required field strength for $\Lambda > 1$ is still far from equipartition (i.e., $\beta \gg 1$). This fact makes Ohmic resistivity essentially irrelevant in determining the vertical extent of the active layer and the accretion rate (since the midplane is already active), while the decisive role is played by AD.

² Note that since $\bar{n} \approx 10^3 n_e$ as read from Figure 2, electrons and other charged species contribute roughly equally to the Ohmic conductivity.

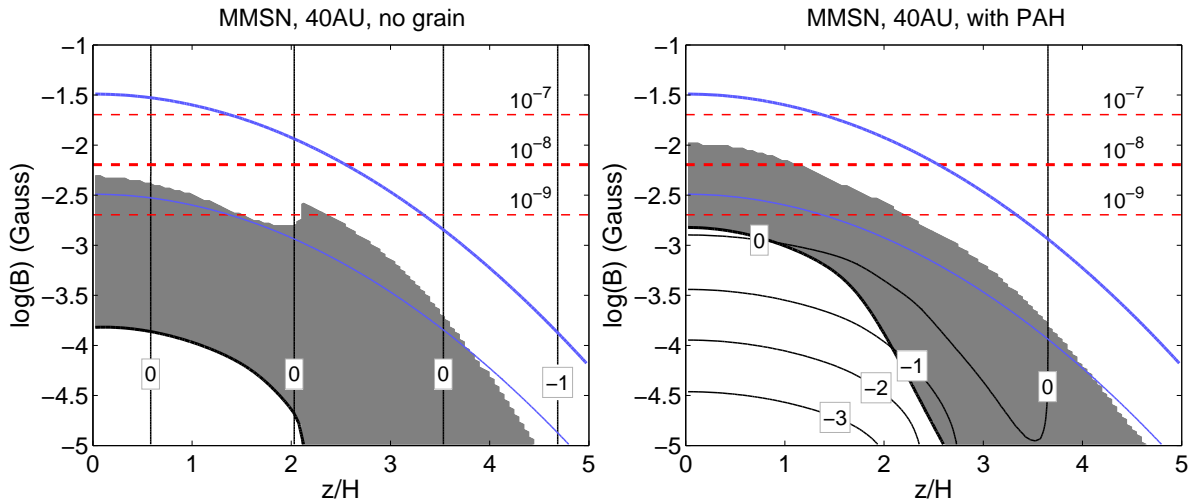


FIG. 3.— MRI permitted region (shaded) in the MMSN model at 40 AU from the grain-free calculation (left) and the calculation including PAHs with $x_{\text{PAH}} = 10^{-8}$ (right). Bold black solid line marks the boundary given by the Ohmic Elsasser number criterion $\Lambda = 1$. Thin black solid lines show contours of constant AD Elsasser number Am , labeled by $\log_{10}(Am)$. Bold and thin blue lines mark plasma accretion rate of 10^{-7} , 10^{-8} and $10^{-9} M_{\odot} \text{ yr}^{-1}$. The red dashed lines indicate the required field strength in the MRI permitted region in order for driving accretion rate of 10^{-7} , 10^{-8} and $10^{-9} M_{\odot} \text{ yr}^{-1}$.

In Figure 3, contours of constant Am are straight lines in the grain free case, as Am is independent of the magnetic field. With the inclusion of tiny grains, we see that near the midplane region, Am increases by 3 orders of magnitude as magnetic field increases. This corresponds to the transition region in Figure 1 with $\beta_i < 1 < \beta_e$. Eventually, at sufficiently strong magnetic field ($\beta_i > 1$), Am becomes independent of magnetic field again. Since $\bar{n} > n_{e0}$, Am is larger in the presence of PAHs than in the grain-free case. Therefore, according to (20), stronger magnetic field is permitted near the disk midplane thanks to the PAHs. According to the strong linear correlation between the Shakura-Sunyaev α parameter and the magnetic field strength (Bai & Stone 2011), an approximate magnetic field strength can be derived if MRI operates in PPDs (Bai 2011)

$$B \approx 2\sqrt{\dot{M}\Omega/H} \approx 1.0\dot{M}_{-8}^{1/2} r_{\text{AU}}^{-11/8} \text{ G}, \quad (21)$$

which assumes the thickness of the active layer to be H on each side, and the second equation assumes one solar mass protostar with MMSN temperature profile. Here \dot{M}_{-8} is accretion rate measured in $10^{-8} M_{\odot} \text{ yr}^{-1}$, r_{AU} is disk radius measured in AU. The required magnetic field strengths for typical observed accretion rates are also illustrated in the Figure. Since stronger field leads to faster accretion, it becomes clear that PAHs are able to make PPDs accrete more rapidly than in the grain-free case.

We note that the above explanation for the enhancement of accretion by tiny grains no longer completely holds in the inner region of PPDs ($\lesssim 10$ AU), where the disk surface density is far above the X-ray penetration depth and accretion is layered. In such situations, the lower boundary of the active layer is determined by both Ohmic resistivity and AD for the two Elsasser number criteria to be satisfied (e.g., see the left panel of Figure 6 in the Appendix). Since Ohmic resistivity is larger in the presence of grains (see the end of Section 2), accre-

tion is thus less efficient than the grain-free case. On the other hand, when PAHs are sufficiently abundant, the increase in Ohmic resistivity is bounded ($\lesssim 10^3$) since conductivity is dominated by the charged PAHs rather than electrons, and the reduction in accretion rate is in general no more than the case with $0.1 \mu\text{m}$ grains (see the next subsection).

3.3. Parameter Study

A more quantitative estimate of the disk accretion rate is discussed in Bai (2011) (see their Section 4.3). The predicted accretion rate \dot{M} is based on the hypothesis that MRI tends to arrange the field configuration to maximize the rate of angular momentum transport, and is optimistic. To demonstrate the role of tiny grains more extensively, we perform our calculations for both the MMSN model and the more massive Desch's disk model at a wide range of disk radii from 1 AU to 100 AU, and consider PAH abundances of $x_{\text{PAH}} = 10^{-9}$, 10^{-8} (fiducial) and 10^{-7} . In addition, we conduct one calculation with cosmic-ray ionization turned off at $x_{\text{PAH}} = 10^{-8}$ for both disk models. In Figure 4, we show the predicted \dot{M} as a function of disk radius for all our calculations. This Figure is to be compared with Figure 4 of Bai (2011), who considered the cases with $0.1 \mu\text{m}$ and $1 \mu\text{m}$ grains. We see that the inclusion of tiny grains makes the predicted \dot{M} comparable to that with solar abundance $0.1 \mu\text{m}$ grains at 1 AU, which is one to two orders magnitude smaller than the grain-free case. However, at larger disk radii, tiny grains promote accretion compared with sub-micron grains, with predicted rate that even exceeds the grain-free case. Below we discuss the effect of PAHs in more detail.

We find that whenever the active layer extends to the disk midplane (the gray area touches the vertical axis in Figure 3, which makes the Ohmic resistivity irrelevant), the predicted \dot{M} in the presence of PAHs exceeds the grain-free case, and the reason is simply due to the

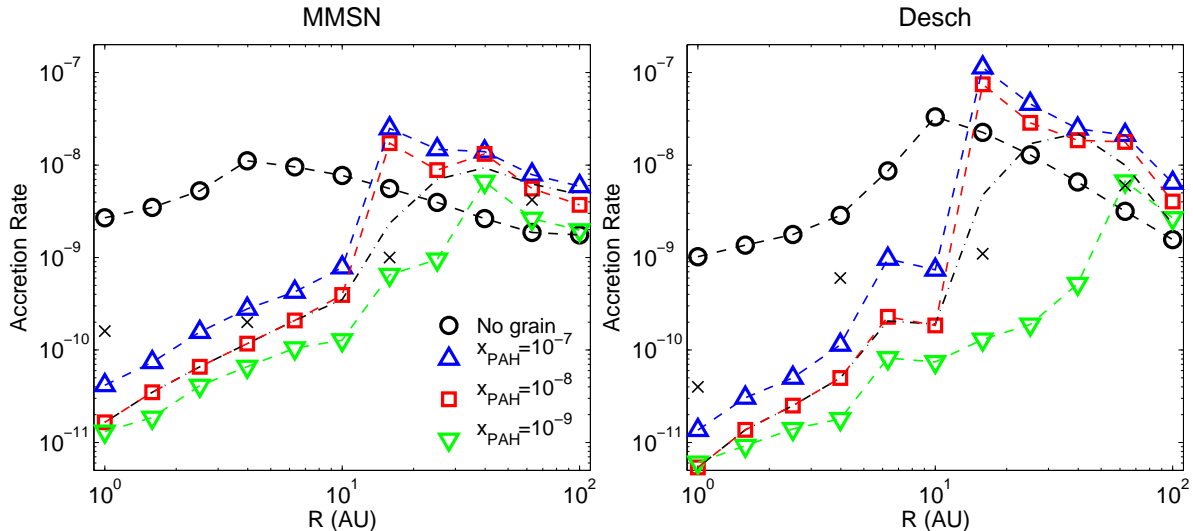


FIG. 4.— Optimistically predicted accretion rate as a function of disk radius for the MMSN disk (left) and the Desch’s disk (right) models. In each panel, we show results from grain-free calculations (black circles) and calculations with various PAH abundances as indicated in the legend. For $x_{\text{PAH}} = 10^{-8}$, we also show the results from calculations without cosmic-ray ionization in the black dash-dotted line. The cross symbols in each panel denote results from the same set of calculations at selected radii but with $x_{\text{PAH}} = 10^{-11}$.

reduction of AD coefficients as discussed in the previous two subsections. This occurs at disk radii $r \gtrsim r_{\text{trans}} \approx 15$ AU for $x_{\text{PAH}} = 10^{-7}$ and 10^{-8} , and for $r \gtrsim r_{\text{trans}} \approx 40$ AU for $x_{\text{PAH}} = 10^{-9}$. Inside the transition radius r_{trans} , accretion is layered and the predicted \dot{M} is well below that in the grain-free case due to Ohmic resistivity as discussed at the end of the previous subsection. The increase in predicted \dot{M} near r_{trans} is very sharp, which is closely related to dependence of Am on magnetic field strength shown in Figure 1, and is discussed in more detail in the Appendix.

An interesting and counterintuitive fact is that higher PAH abundance leads to faster accretion at all disk radii. This fact can be understood as follows. First of all, near the base of the active layer, we find that charged grain abundance is so much higher than the electron abundance that the Ohmic resistivity is determined by charged grains rather than electrons (i.e., $\theta \gtrsim 1$). Therefore, even the abundance of free electrons rapidly decreases with increasing x_{PAH} , the Ohmic resistivity approximately stays at the same level (while still much larger than the grain-free resistivity). Secondly, as we mentioned in the discussion after equation (19), the grain ionization level n_{gr}^{\pm}/n_H increases weakly with the total grain abundance x_{PAH} . This fact reduces both the Ohmic resistivity and the AD coefficient, which leads to faster accretion. Only at $r \lesssim 1$ AU, and when x_{PAH} is small (10^{-9} or less), does the Ohmic resistivity at the base of the active layer determined by electrons, which produces higher accretion rate than larger x_{PAH} cases.

We see that in the presence of PAHs, the predicted \dot{M} increases with disk radius for $r \lesssim r_{\text{trans}}$ where accretion is layered, and falls off with radius for $r \gtrsim r_{\text{trans}}$ as the disk midplane is activated. Also, larger disk surface density generally leads to smaller \dot{M} in the inner disk when accretion is layered (although not by much), while when the disk midplane becomes active in the outer disk, the Desch’s disk model gives higher \dot{M} . These features are

all consistent with the results presented in Bai (2011), where explanations are offered (see Section 5.1).

In addition, we see in the dash-dotted line of Figure 4 that when cosmic-ray ionization is turned off (since it may be shielded by protostellar winds), the predicted \dot{M} is almost indistinguishable with our fiducial case at the inner 10 AU. The predicted \dot{M} still exceeds that in the grain-free case in the outer disk, with the transition radius r_{trans} slightly larger than that in the fiducial calculation, and the increase in \dot{M} near r_{trans} is less sharp. Beyond r_{trans} , the accretion rate reduction is generally within a factor of 2 of the fiducial result. These results are all consistent with Bai (2011), where it is shown and discussed that the deeper-penetrating cosmic-ray ionization does not substantially enhance the accretion rate compared with the X-ray ionization (see Section 5.2).

Finally, we emphasize that the existence of r_{trans} and the fact that \dot{M} increases with x_{PAH} holds only when PAHs are sufficiently abundant ($x_{\text{PAH}} \gtrsim 10^{-9}$). For comparison, we also show in Figure 4 with cross symbols the predicted accretion rate at selected disk radii with $x_{\text{PAH}} = 10^{-11}$. At small radius of ~ 1 AU, the predicted \dot{M} is well above the cases with higher PAH abundances. This is because the free electrons is much more abundant so that electron conductivity dominates grain conductivity, and gives smaller resistivity. The disk midplane becomes active at $r \gtrsim 15$ AU, but we do not find the sharp jump in the predicted \dot{M} as in the case with higher PAH abundances, and the predicted accretion rate is also smaller by a factor of up to 100. This is because x_{PAH} is so small that the grain number density is well below n_e (so $\bar{n}/n_e \approx 1$) and the effects we discussed before no longer apply.

The role of PAHs in PPDs has been recently studied by Perez-Becker & Chiang (2011a). Besides the fact that they used a more stringent criterion for AD to suppress the MRI, the Am values they obtained were largely underestimated because they adopted the sim-

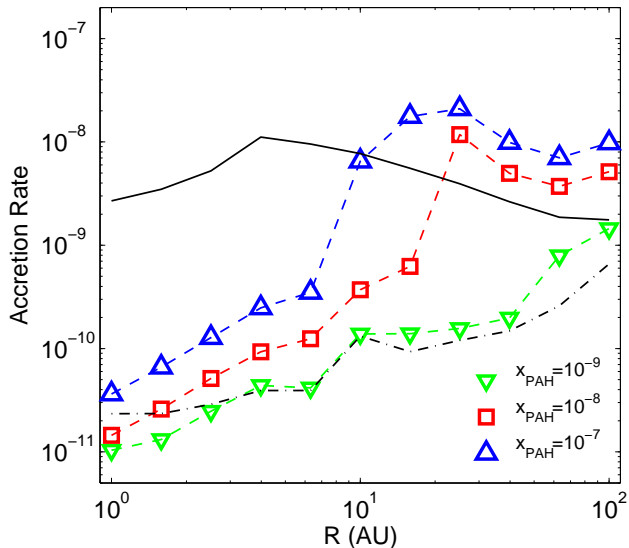


FIG. 5.— Optimistically predicted accretion rate as a function of disk radius for the MMSN disk with two populations of grains: $0.1\mu\text{m}$ grains with fixed mass fraction of 1% and PAHs with abundance $x_{\text{PAH}} = 10^{-9}, 10^{-8}$ and 10^{-7} . Comparison is made to the grain-free case (black solid) and case with single population of $0.1\mu\text{m}$ grains (black dash-dotted).

ple formulae (2) without taking into account the contribution from grains. This has led them to conclude that the presence of PAHs makes the MRI too inefficient to drive rapid accretion at all disk radii, although as we have shown that PAHs in fact promote accretion in the outer disk, and at all disk radii the predicted accretion rate generally increases with PAH abundance. Our findings are subsequently confirmed in their follow-up work (Perez-Becker & Chiang 2011b) with corrected grain conductivities.

3.4. Effect of Grain Size Distribution

Our study so far have considered only single-species of grains. In reality, tiny grains coexist with larger grains with the latter dominates the grain mass (but not necessarily abundance). To justify our findings in a more realistic context, we conduct another set of calculations with two populations of grains. Besides the PAH population with $x_{\text{PAH}} = 10^{-9}, 10^{-8}$ and 10^{-7} that contributes a negligible amount of mass, we add the second population of $0.1\mu\text{m}$ grains with fixed mass fraction of 1%. In Figure 5, we show the predicted accretion rate as a function of disk radius in the same way as Figure 4. For comparison, we also plot the predicted \dot{M} in the grain-free case (black solid) and the pure $0.1\mu\text{m}$ grain case (black dash-dotted) taken from Bai (2011). We see that at fixed PAH abundance with $x_{\text{PAH}} \gtrsim 10^{-8}$, the predicted \dot{M} with two grain populations is very close to that in our previous calculations with a single PAH population, and it behaves as if the $0.1\mu\text{m}$ grains do not exist. In particular, the sharp enhancement of accretion beyond the transition radius is clearly present, and the predicted \dot{M} increases with x_{PAH} . At $x_{\text{PAH}} = 10^{-9}$, the situation is marginal: with the addition of $0.1\mu\text{m}$ grains, the signature of sharp transition is less obvious, which occurs at $r_{\text{trans}} \sim 60$

AU, and beyond r_{trans} the predicted \dot{M} is still less than that in the grain-free case. In fact, the behavior of the two-population calculation at $x_{\text{PAH}} = 10^{-9}$ roughly lies in between the two single-population limits.

Our results are consistent with chemistry studies by Bai & Goodman (2009) which indicate that different grain populations tend to behave independently. Therefore, the outcome of a size distribution of grains is mainly determined by the grain population that dominates the recombination process. Bai & Goodman (2009) found that the controlling parameter of the recombination lies in between the total surface area and the grain abundance weighted by linear size. As an approximation we weigh the grain abundance by $a^{3/2}$ and find that PAHs and $0.1\mu\text{m}$ sized grains contribute roughly equally to the recombination process when $x_{\text{PAH}} \sim 3 \times 10^{-9}$, consistent with our findings discussed in the previous paragraph.

In sum, the effect of tiny grains studied in this paper is approximately independent of the presence of larger grains, and we quote $x_{\text{PAH}} = 10^{-9}$ as the critical tiny grain abundance above which enhancement of accretion is possible in the outer regions of PPDs.

4. SUMMARY AND DISCUSSION

Tiny grains are important charge carriers in weakly ionized gas and strongly affect the non-ideal MHD effects when their abundance is above the ionization fraction. We generalize the commonly used simple expressions for non-ideal MHD diffusion coefficients (2) to incorporate the effect of charged tiny grains. We show that at sufficiently small ionization level, tiny grains become the dominant charge carriers, and the non-ideal MHD diffusion coefficients behave very differently from the grain-free case. The Ohmic conductivity is dominated by charged grains rather than electrons when \bar{n} exceeds about $10^3 n_e$. In the AD regime (strong magnetic field), Hall and AD coefficients are strongly reduced by a factor of about $(\bar{n}/n_e)^2$ relative to those in the Ohmic regime (weak magnetic field), and for sufficiently large \bar{n}/n_e , Hall dominated regime diminishes.

We study the role of tiny grains on the MRI driven accretion in PPDs, and find that novel behaviors occur when the tiny grains are sufficiently abundant with $x_{\text{PAH}} \gtrsim 10^{-9}$, regardless of whether larger grains are present or not. At the inner disk where accretion is layered, the predicted accretion rate in the presence of tiny grains is one to two orders of magnitude less than the grain-free case due to increased Ohmic resistivity, but is similar to or higher than that with solar-abundance $0.1\mu\text{m}$ grains. A sharp increase in the predicted \dot{M} occurs at the transition radius $r_{\text{trans}} \approx 15$ AU (in the fiducial model) where the disk midplane becomes active, making Ohmic resistivity irrelevant to the accretion rate. Quite unexpectedly, we find that at $r \gtrsim r_{\text{trans}}$, tiny grains make accretion even more rapid than the grain-free case. Moreover, our predicted accretion rate increases with PAH abundance. These results are due to that at large PAH abundance, ionization-recombination balance makes \bar{n} orders of magnitude larger than n_e , and even exceeds the grain-free electron density n_{e0} at disk midplane. These facts prevent Ohmic resistivity from rapidly increasing as x_{PAH} increases, reduce the dissipation by AD, thus

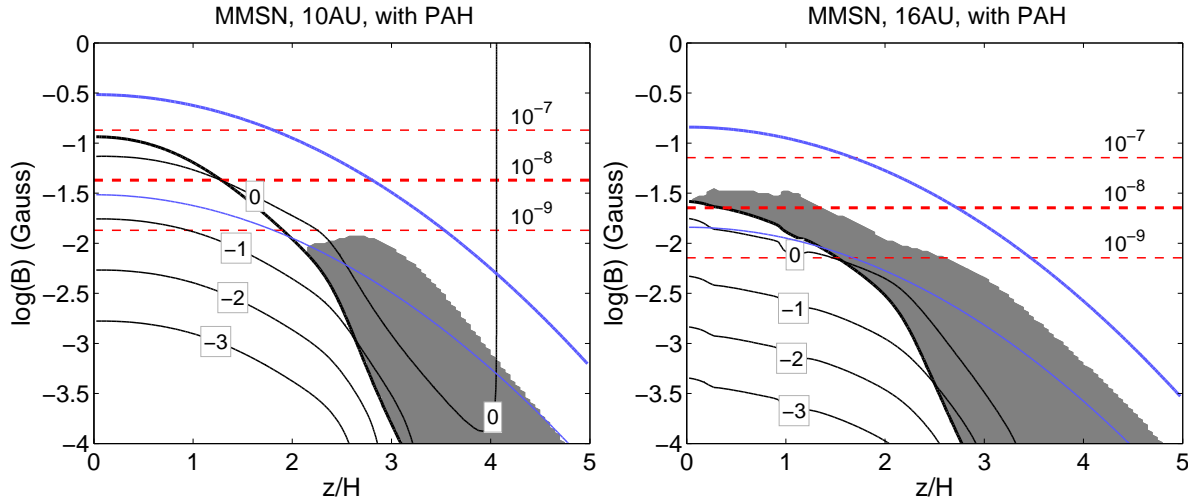


FIG. 6.— Same as Figure 3, but for MRI permitted region (shaded) in the MMSN model at 10 AU (left) and 16 AU (right) from calculations with PAHs at $x_{\text{PAH}} = 10^{-8}$.

facilitate the active layer to extend deeper into the disk midplane and permit stronger MRI turbulence. Our results highlight the importance of evaluating the full conductivity tensor in the calculation of the non-ideal MHD diffusion coefficients rather than using the simple grain-free formulae (2).

We emphasize that the effects studied in this paper mainly apply to tiny grains ($\lesssim 0.01\mu\text{m}$), and when they are sufficiently abundant ($x_{\text{PAH}} \gtrsim 10^{-9}$). For grains larger than $0.1\mu\text{m}$, their abundance is at most 3×10^{-12} per H_2 molecule (for having 1% of mass), which is orders of magnitude smaller than 10^{-9} . The reduction of AD coefficient also exist for these relatively larger grains, as can be seen in the bottom panels of Figure 3 in Bai (2011), but its effect is much more limited than the tiny grain case. When large grains and tiny grains coexist, the effect of large grains becomes negligible if $x_{\text{PAH}} > 10^{-9}$.

Although tiny grains strongly enhance PPD accretion in the outer disk, the situation at the inner disk is still similar to the case with $0.1\mu\text{m}$ grains (Bai 2011), with predicted accretion rate much less than the typical value of $10^{-8}M_{\odot} \text{yr}^{-1}$ as inferred from observations (Hartmann et al. 1998). The recently proposed far ultraviolet (FUV) ionization scenario does not provide large accretion rate in the inner disk either due to the small penetration depth of FUV photons (Perez-Becker & Chiang 2011b). Therefore, either additional ionization sources has to make the MRI more efficient than the X-rays and FUV photons (candidate may include energetic protons from the protostars (Turner & Drake 2009)), or additional mechanism such

as magnetized wind (Salmeron et al. 2007) operates to provide the angular momentum transport in the inner disk.

In the case of transitional disks characterized by inner holes or gaps (Calvet et al. 2002; Espaillat et al. 2007), we note that the observationally inferred outer boundary of the holes or gaps is typically at a few tens of AU (Hughes et al. 2009; Kim et al. 2009), which is generally greater than r_{trans} in our models with PAHs. Therefore, the enhancement of accretion by tiny grains works effectively for transitional disks, and X-ray driven MRI with PAHs is able to feed the inner hole /gap at the (optimistic) rate of about $10^{-8}M_{\odot} \text{yr}^{-1}$. This is sufficient to account for the observed accretion rate in transitional disks (Najita et al. 2007; Sicilia-Aguilar et al. 2010), with the accreting gas fed from the outer disk flowing through the hole / gap possibly guided by multiple planets (Chiang & Murray-Clay 2007; Perez-Becker & Chiang 2011a; Zhu et al. 2011).

X.-N.B thanks Jim Stone and Jeremy Goodman for carefully reading the manuscript with comments, and Bruce Draine for useful discussions on PAHs. Comments from Daniel Perez-Becker and the referee, Eugene Chiang, are especially acknowledged which lead to several improvements to this work. This work is supported by NASA Headquarters under the NASA Earth and Space Science Fellowship Program Grant NNX09AQ90H awarded to X.N.B.

APPENDIX

MIDPLANE ACTIVATION AT TRANSITION RADIUS

It has been shown in Figure 4 and discussed in Section 3.3 that near the transition radius r_{trans} where the disk midplane becomes active, the predicted accretion rate \dot{M} increases sharply with radius, from well below the grain-free rate at $r < r_{\text{trans}}$ to a factor of several higher at $r > r_{\text{trans}}$. We discuss the activation of the midplane by the MRI in this Appendix and explain the sharp dependence of \dot{M} on disk radius near r_{trans} .

Figure 6 shows the MRI permitted region in our fiducial model at 10 and 16 AU between which lies the transition radius. We see from this plot that much stronger magnetic field is permitted in the disk midplane once it is activated,

which is the cause of the big jump in \dot{M} .

Looking more closely into the sharp transition, we find it is related to the dependence of the AD Elsasser number Am on the magnetic field strength. We have shown in Figure 1 that η_A depends on the magnetic field quadratically in weak ($\beta_e < 1$) and strong ($\beta_i > 1$) field regimes as commonly considered, but at the intermediate regime with $\beta_i < 1 < \beta_e$, η_A behaves similarly as η_O and does not depend on the magnetic field strength. Consequently, the contours of Ohmic and AD Elsasser numbers Λ and Am are nearly parallel to each other, and both shapes are close to (near the midplane) or slightly steeper (near the surface) than the contours of constant β , as can be seen in Figure 6. In the mean time, an increase of ionization level (as one moves to outer radius) brings down the Am and Λ contours relative to the β contour in a wide range of disk heights. Then, according to our criteria for the MRI to operate ($\Lambda > 1$ and $\beta > \beta_{\min}(Am)$), once the ionization level in the disk reaches some critical degree (i.e., left panel of Figure 6), a further increase in ionization would suddenly make both criteria satisfied simultaneously across the midplane (i.e., right panel of Figure 6), leading to the sharp transition.

REFERENCES

- Acke, B. & van den Ancker, M. E. 2004, *A&A*, 426, 151
 Bai, X. & Stone, J. M. 2011, *ApJ*, in press (arXiv:1103.1380)
 Bai, X.-N. 2011, *ApJ*, accepted
 Bai, X.-N. & Goodman, J. 2009, *ApJ*, 701, 737
 Balbus, S. A. 2011, in *Physical Processes in Circumstellar Disks and Young Stars*, ed. P. Garcia, University of Chicago Press (arXiv:0906.0854)
 Balbus, S. A. & Hawley, J. F. 1991, *ApJ*, 376, 214
 Calvet, N., D'Alessio, P., Hartmann, L., Wilner, D., Walsh, A., & Sitko, M. 2002, *ApJ*, 568, 1008
 Chiang, E., & Murray-Clay, R. 2007, *Nature Physics*, 3, 604
 D'Alessio, P., Calvet, N., & Hartmann, L. 2001, *ApJ*, 553, 321
 Desch, S. J. 2007, *ApJ*, 671, 878
 Draine, B. T. & Sutin, B. 1987, *ApJ*, 320, 803
 Espaillat, C., Calvet, N., D'Alessio, P., Hernández, J., Qi, C., Hartmann, L., Furlan, E., & Watson, D. M. 2007, *ApJ*, 670, L135
 Gammie, C. F. 1996, *ApJ*, 457, 355
 Geers, V. C., Augereau, J., Pontoppidan, K. M., Dullemond, C. P., Visser, R., Kessler-Silacci, J. E., Evans, II, N. J., van Dishoeck, E. F., Blake, G. A., Boogert, A. C. A., Brown, J. M., Lahuis, F., & Merín, B. 2006, *A&A*, 459, 545
 Geers, V. C., van Dishoeck, E. F., Visser, R., Pontoppidan, K. M., Augereau, J.-C., Habart, E., & Lagrange, A. M. 2007, *A&A*, 476, 279
 Hartmann, L., Calvet, N., Gullbring, E., & D'Alessio, P. 1998, *ApJ*, 495, 385
 Hayashi, C. 1981, *Progress of Theoretical Physics Supplement*, 70, 35
 Hughes, A. M., et al. 2009, *ApJ*, 698, 131
 Kim, K. H., et al. 2009, *ApJ*, 700, 1017
 Najita, J. R., Strom, S. E., & Muzerolle, J. 2007, *MNRAS*, 378, 369
 Oliveira, I., Pontoppidan, K. M., Merín, B., van Dishoeck, E. F., Lahuis, F., Geers, V. C., Jørgensen, J. K., Olofsson, J., Augereau, J., & Brown, J. M. 2010, *ApJ*, 714, 778
 Oppenheimer, M. & Dalgarno, A. 1974, *ApJ*, 192, 29
 Perez-Becker, D. & Chiang, E. 2011a, *ApJ*, 727, 2
 —. 2011b, *ApJ*, 735, 8
 Salmeron, R. & Wardle, M. 2003, *MNRAS*, 345, 992
 Salmeron, R., Königl, A., & Wardle, M. 2007, *MNRAS*, 375, 177
 Sicilia-Aguilar, A., Henning, T., & Hartmann, L. W. 2010, *ApJ*, 710, 597
 Turner, N. J., & Drake, J. F. 2009, *ApJ*, 703, 2152
 Turner, N. J., Sano, T., & Dziourkevitch, N. 2007, *ApJ*, 659, 729
 Umebayashi, T. & Nakano, T. 1990, *MNRAS*, 243, 103
 van Boekel, R., Waters, L. B. F. M., Dominik, C., Bouwman, J., de Koter, A., Dullemond, C. P., & Paresce, F. 2003, *A&A*, 400, L21
 Wardle, M. 1999, *MNRAS*, 307, 849
 Wardle, M. 2007, *Ap&SS*, 311, 35
 Zhu, Z., Nelson, R. P., Hartmann, L., Espaillat, C., & Calvet, N. 2011, *ApJ*, 729, 47